Geochemistry Geophysics Geosystems G3

Article
Volume 11, Number 10
6 October 2010
Q10001, doi:10.1029/2010GC003243
ISSN: 1525-2027

Published by AGU and the Geochemical Society

Numerical investigations of apatite $^4He/^3He$ thermochronometry

K. A. Farley
Division of Geological and Planetary Sciences, California Institute of Technology, MS 170-25, Pasadena, California 91125, USA (farley@gps.caltech.edu)

D. L. Shuster
Berkeley Geochronology Center, 2455 Ridge Road, Berkeley, California 94709, USA

E. B. Watson
Department of Earth and Environmental Sciences, Rensselaer Polytechnic Institute, Troy, New York 12180-3590, USA

K. H. Wanser
Department of Physics, California State University, Fullerton, California 92831, USA

G. Balco
Berkeley Geochronology Center, 2455 Ridge Road, Berkeley, California 94709, USA

[1] Apatite $^4He/^3He$ thermochronometry has the potential to constrain cooling histories for individual samples provided that several presently untested assumptions are valid. Here we simulate the sensitivity of $^4He/^3He$ spectra to assumptions regarding geometric model, crystallographic anisotropy, broken grain terminations, parent nuclide zonation, and the accuracy of results obtained from analyses of aggregates of multiple crystals. We find that $^4He/^3He$ spectra obtained from a cylinder with isotropic diffusion are almost indistinguishable from those obtained from an equivalent sphere with an equivalent initial ^4He distribution. Under similar conditions anisotropic diffusion from the cylinder can greatly bias $^4He/^3He$ spectra, but only if diffusion is >10 times faster in the axial than the radial direction. Existing data argue against anisotropy of this magnitude. We find that analysis of apatites with broken terminations will also bias $^4He/^3He$ spectra, but not greatly so. In contrast, we find that zonation of a factor of 3 in parent nuclide concentration produces $^4He/^3He$ spectra that deviate substantially from the homogeneous model. When parent nuclides are highly concentrated near the grain rim and/or cooling is fast, the resulting $^4He/^3He$ spectra will be readily identified as aberrant. However, more subtle zonation, higher concentrations in the grain interior, or samples that have cooled slowly regardless of zonation style can yield $^4He/^3He$ spectra that look acceptable but will lead to inaccurate thermochronometric interpretation if parent homogeneity is assumed. Finally, we find that analysis of an aggregate of crystals with identical ^4He distributions can yield $^4He/^3He$ spectra (and diffusion Arrhenius arrays) that are very different from those that would be obtained on the individual crystals if even small variations in He diffusion exist among the grains. Overall, our observations suggest that modeling tools that assume spherical geometry and isotropic diffusion are appropriate for interpreting apatite $^4He/^3He$ spectra. However, it is essential to analyze only individual crystals and to assess the degree of parent nuclide zonation in those crystals.

Components: 8600 words, 7 figures.

Keywords: geochronology; He dating; $^4He/^3He$.

Index Terms: 1140 Geochronology: Thermochronology; 1115 Geochronology: Radioisotope geochronology.

Received 27 May 2010; **Revised** 2 August 2010; **Accepted** 18 August 2010; **Published** 6 October 2010.

Farley, K. A., D. L. Shuster, E. B. Watson, K. H. Wanser, and G. Balco (2010), Numerical investigations of apatite ^{4}He/^{3}He thermochronometry, *Geochem. Geophys. Geosyst.*, *11*, Q10001, doi:10.1029/2010GC003243.

1. Introduction

[2] Over the last decade both the mechanistic underpinnings and the applications of apatite (U-Th)/He dating have expanded greatly. The method is based on the ingrowth of ^{4}He from α decay of U and Th series nuclides and ^{147}Sm, which are typically found at ppm levels in apatite and commonly assumed to have a uniform spatial distribution. Laboratory diffusion experiments indicate a He closure temperature of about 60–70°C for typical apatites [*Farley*, 2000; *Wolf et al.*, 1996a], increasing with the abundance of radiation damage in the apatite [*Shuster et al.*, 2006]. A central premise of the method is that the observed ^{4}He concentration arises from the competing effects of radiogenic ingrowth and diffusive loss integrated over the time-temperature history of the sample. Thus cooling paths can be constrained by a crystal's (U-Th)/He age [*Wolf et al.*, 1998].

[3] In most circumstances the resulting cooling paths are nonunique. For example, a volcanic apatite would yield a (U-Th)/He age of 2 Ma if it was erupted at that time and never experienced He diffusion. An identical age would be obtained on an intrusive apatite residing at ~70°C for 100 Ma, during which production and diffusion achieve a steady state [*Wolf et al.*, 1998]. In most geologic applications of low-temperature thermochronometry the problem of nonuniqueness is overcome by using age-elevation relationships [*Fitzgerald et al.*, 1995; *Wagner and Reimer*, 1972; *Wolf et al.*, 1996b] that provide information on relative cooling histories of samples that are spatially related to one another. In this case the quantity usually being constrained is the exhumation rate of a package of rocks through isotherms rather than the cooling path of any one rock.

[4] An additional constraint on the permissible cooling paths of a single sample lies in the shape (rather than just the integral) of the ^{4}He concentration distribution (Figure 1a). Returning to the example described above, the ^{4}He concentration in the volcanic grain would be uniform except for the effects of α ejection [*Farley et al.*, 1996], while the intrusive grain at steady state would have an extremely rounded profile (Figure 1a). Numerical modeling confirms that the ^{4}He concentration profile is a very rich source of information on an apatite's cooling history [*Shuster and Farley*, 2004].

[5] At present there are no microbeam or laser-based techniques with adequate spatial resolution and sensitivity to measure this profile in apatite, although some success has now been achieved with larger spot sizes [*Boyce and Hodges*, 2005]. As an alternative, *Shuster et al.* [2004] proposed an indirect approach referred to as ^{4}He/^{3}He thermochronometry. Irradiation with ~200 MeV protons creates a uniform distribution of ^{3}He within a crystal without disturbing the ^{4}He distribution. The irradiated sample is then thermally degassed in a series of steps in which the evolved He is measured. The result is a ^{4}He/^{3}He spectrum, i.e., a plot of the ^{4}He/^{3}He ratio of each step (normalized to the ^{4}He/^{3}He ratio of the bulk sample) plotted as a function of the cumulative fraction of ^{3}He released up to and including that step (ΣF^3He).

[6] The ^{4}He/^{3}He spectrum can either be formally inverted for the ^{4}He profile, or more commonly, the spectrum can be compared with spectra forward modeled for specific time-temperature paths using a He diffusion kinetic model [*Shuster and Farley*, 2005]. The ^{4}He/^{3}He method is sensitive across the entire temperature range from ~30°C to ~90°C. Recent efforts have applied ^{4}He/^{3}He thermochronometry to constrain the timing and rates of glacial erosion [*Shuster et al.*, 2005], fluvial erosion [*Schildgen et al.*, 2010], and normal faulting [*Colgan et al.*, 2008].

[7] Over the last several years we have worked to improve and simplify the ^{4}He/^{3}He analytical method, and have analyzed a fairly large number of apatites. While many samples, such as those described above, yield sensible ^{4}He/^{3}He spectra, others do not. In this work we identify several factors that can (and several that cannot) be responsible for the anomalous spectra. The results obtained are directly relevant for understanding ^{4}He/^{3}He spectra,

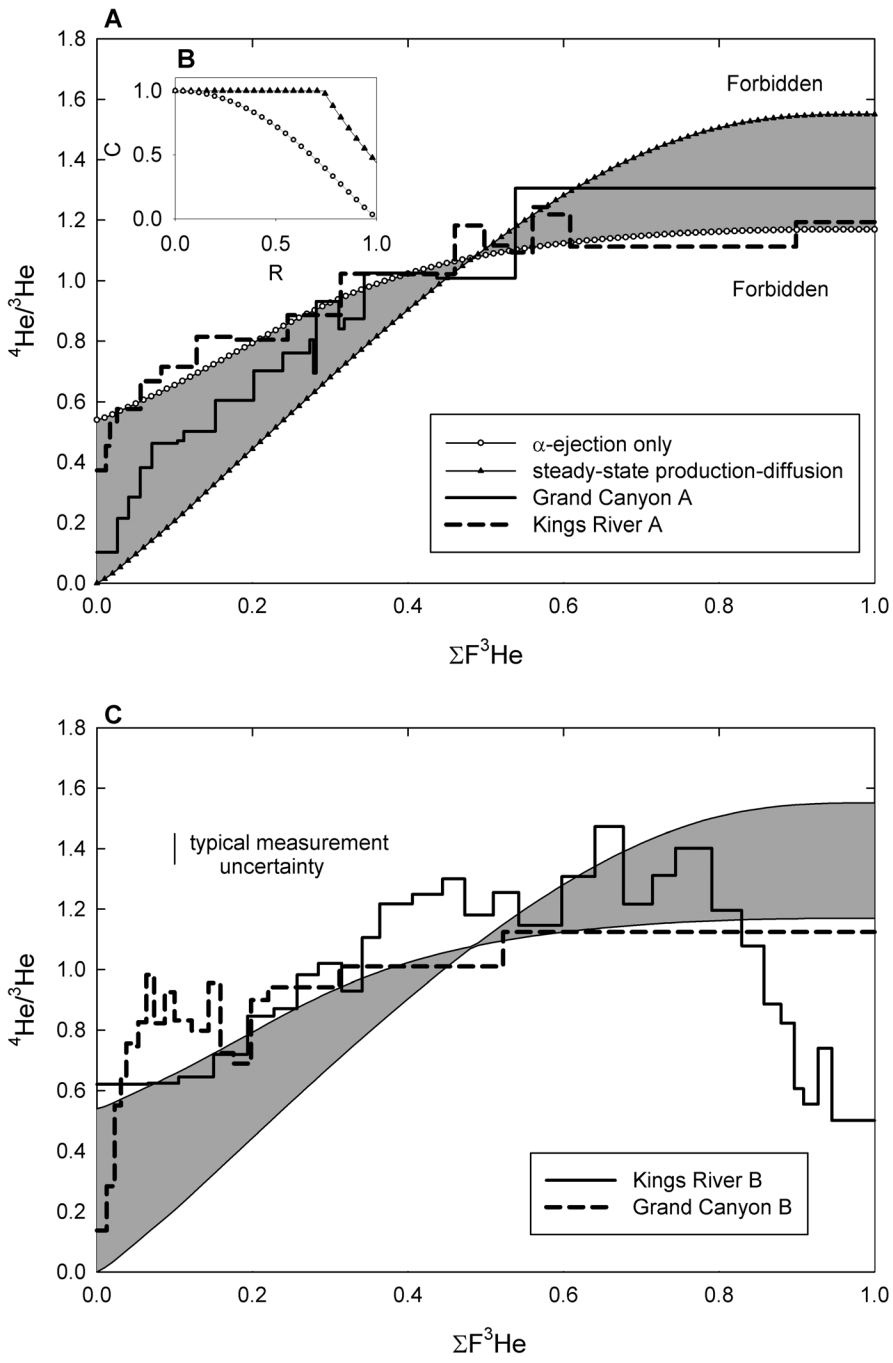

Figure 1. Limiting $^4He/^3He$ spectra and examples. (a) Spectra for the two limiting cases of α ejection-only and production-diffusion-α ejection steady state evolved from (b) the limiting concentration profiles (C, normalized concentration; R, normalized radial coordinate). All $^4He/^3He$ spectra that conform to assumptions (see section 1 for details) must lie within uncertainty of the shaded region and not in the regions labeled "forbidden." Also shown in Figure 1a are two spectra that plot within error of the allowed region. (c) Two obviously anomalous measured $^4He/^3He$ spectra (sample and data details in Data Set S1). These spectra were measured on multiple grain aliquots. Note that measured spectra are plotted as a series of steps reflecting the amount of gas released in each step, whereas the model curves here are continuous curves that would apply to very small steps. For clarity the uncertainties on measured data are not shown, but a typical 1 σ uncertainty estimate is indicated in Figure 1c.

and more broadly, are useful for evaluating some of the basic assumptions underlying apatite (U-Th)/He dating.

[8] ^{4}He/^{3}He spectra that conform to the assumptions of a uniform distribution of parent nuclides and ^{4}He production-diffusion in a sphere must plot within tight bounds (Figure 1a [*Shuster and Farley*, 2004]). One bound is defined by a sample that has experienced no diffusion whatsoever. If the decay energies were very small, this would simply be a line plotting at a ^{4}He/^{3}He ratio of unity across the full range of ΣF^{3}He. In reality α particles produced in apatite have a range of about 20 μm; this causes a fraction of the α particles produced within 20 μm of the edge of the grain to be ejected [*Farley et al.*, 1996]. The diffusion domain in apatite is the entire crystal [*Farley*, 2000], so this clipped profile is the production function subjected to diffusion (Figure 1b). Thus the "α ejection-only" profile yields one limit to the ^{4}He/^{3}He spectrum produced in an apatite, i.e., one that has experienced no diffusional modification of the ^{4}He distribution. The other bound is dictated by the steady state condition that ^{4}He production and diffusion are precisely balanced. This yields a highly rounded diffusion profile that is independent of diffusivity. (For present purposes we ignore the case of recent "flash" heating, which could produce profiles even more rounded than that arising from steady state production-diffusion). Figure 1a illustrates these bounds for an apatite with a radius of 75 μm and includes the effects of α ejection.

[9] The key point here is that ^{4}He in an apatite accurately described by a spherical diffusion model, with a uniform distribution of parent nuclides and arising solely from production and diffusion, must have a ^{4}He/^{3}He spectrum plotting between these two bounds. An additional expectation arising from these assumptions is that ^{4}He/^{3}He spectra should vary smoothly and should increase monotonically with ΣF^{3}He.

[10] Figure 1a shows examples of two previously unpublished ^{4}He/^{3}He spectra that obey these expectations: one that lies very close to the α ejection-only limit, and another that has apparently experienced more diffusive loss. In contrast to these acceptable profiles, Figure 1c shows previously unpublished ^{4}He/^{3}He spectra for two samples that plot in the forbidden region: one with a "hump" at low ΣF^{3}He, and the other with a strong deviation to low ratios at high ΣF^{3}He. The goal of this paper is to identify what might cause these unanticipated spectra. Factors that we will consider are sensitivity to the assumed geometric model (sphere, cylinder), possible diffusional anisotropy in apatite, analysis of recently broken crystals, analysis of aliquots of multiple crystals among which He diffusivity varies, and U-Th-Sm zonation.

2. General Mathematical Approximations

[11] In the scenarios considered below we simulate ^{4}He/^{3}He spectra under various assumptions. For these simulations we use approximations for the solution to the diffusion equation for the sphere and for the finite cylinder. For the cylinder, we adopt the analytical approximations given by *Watson et al.* [2010]. While in most cases we consider isotropic diffusion, in several instances we require the more general formulae for anisotropic diffusion. The cylinder has height h and radius a, with radial diffusion coefficient D_{11} and axial diffusion coefficient D_{33}. We use the dimensionless release coordinates:

$$y_1(t) = \int_0^t \frac{D_{11}(t')}{a^2}dt' \; y_3(t) = \int_0^t \frac{D_{33}(t')}{h^2}dt'$$

where the subscripts on y refer to the radial (1) or axial (3) dimension, t is the interval over which diffusion has occurred and t' is the integration variable. From *Watson et al.* [2010], the fraction F of helium released from the anisotropic cylinder starting with an initially uniform concentration is:

$$F(y_1, y_3) = F_1(y_1) + F_3(y_3) - F_1(y_1)F_3(y_3)$$

where F_1 and F_3 are equivalent to the fractional losses for the infinite cylinder and infinite slab, respectively, and are approximated by:

$$F_1 \cong 4\sqrt{\frac{y_1}{\pi}} - y_1 - \frac{y_1^{3/2}}{3\sqrt{\pi}} - 0.244122y_1^2 \qquad \textit{valid for } F_1 < 0.78$$

$$F_1 \cong 1 - \frac{4}{\alpha_1^2}e^{-\alpha_1^2 y_1} \qquad \textit{valid for } F_1 \geq 0.78$$

where $\alpha_1 = 2.404826$.

$$F_3 \cong 4\sqrt{\frac{y_3}{\pi}} \qquad \textit{valid for } F_3 < 0.52$$

$$F_3 \cong 1 - \frac{8}{\pi^2}e^{-\pi^2 y_3} \qquad \textit{valid for } F_3 \geq 0.52$$

In the case of the sphere of radius r, we use the approximations for fractional release F given by *Fechtig and Kalbitzer* [1966]:

$$F \cong \frac{6}{\sqrt{\pi}}\sqrt{y} - 3y \qquad \textit{valid for } F < 0.85$$

$$F \cong 1 - \frac{6}{\pi^2}e^{-\pi^2 y} \qquad \textit{valid for } F \geq 0.85$$

Where the release coordinate y for the sphere is given by:

$$y(t) = \int_0^t \frac{D(t')}{r^2}dt'$$

These equations allow computation of the fractional loss of diffusant from a sphere or cylinder subjected to a diffusion interval characterized by release coordinate y (for the sphere) or y_1, y_3 (for the anisotropic cylinder). These equations also apply to a simulated step heating experiment, in which there are a series of such intervals which progressively degas the sample. By subtracting the cumulative yield obtained in heating step $i - 1$ from the cumulative yield obtained in heating step i, we can compute the fractional yield F_i associated with degassing step i. Note here that subscript i refers to step number and should not be confused with the direction−related release fractions F_1 and F_3.

[12] To generate the synthetic ^{4}He/^{3}He spectrum that would be obtained from a step heat experiment, we first compute the table of F_i values starting with a uniform initial distribution. We use an arbitrary "step heating schedule" (in reality, a series of monotonically increasing release coordinates) that insures an appropriate distribution of fractional yield values up to near-total degassing (>99%). This simulates the release of the uniformly distributed ^{3}He.

[13] To simulate the initially diffusionally modified ^{4}He distribution, we simply add an additional step prior to the schedule used for ^{3}He. The release coordinate for this "zeroth" step is chosen so as to produce a specified fractional yield F_o. We refer to this as "prior degassing." The table of F_i values for the remainder of the schedule is computed using the same approximations as for ^{3}He. However, because there was prior degassing, we need to adjust the fractional yield data accordingly, i.e., if we are simulating 10% prior degassing, then the total yield in the simulation is 0.9 rather than unity, so we scale each computed yield upward by a factor $1/(1 - F_o)$. Note that the result of this approach is a purely diffusive ^{4}He profile, rather than one arising from production and diffusion. The two helium isotopes are assumed to have identical diffusivity [*Shuster et al.*, 2004].

[14] We also employ a modified version of the program Cylmod described by *Watson et al.* [2010]. This program (CylmodE) provides a numerical solution to anisotropic diffusion from a finite cylinder starting with an α ejection distribution, an initial condition which currently available analytical solutions cannot accommodate. This distribution is approximated by a linear decrease in concentration from unity at depths >20 μm from the nearest edge, to a value of 0.45 on the grain surface. For nodes that lie within 20 μm of both radial and axial surfaces, the computation uses the distance to the nearest edge.

[15] Last, we use a numerical He production-diffusion model [*Schildgen et al.*, 2010] to compute ^{4}He/^{3}He spectra arising from grains with a spatially heterogeneous (but only radially varying) distribution of parent nuclides, here referred to as zoned in effective U (eU). This model generates the ^{4}He production profile from an assumed eU distribution in a spherical domain including α ejection, then calculates the ^{4}He/^{3}He spectrum arising from that distribution using a finite difference solution to the spherical diffusion equation.

[16] For all of these approaches we obtain a ^{4}He/^{3}He spectrum with a finite number of discrete steps rather than a continuum of points. In this sense the models mimic a ^{4}He/^{3}He spectrum obtained in the laboratory. For both laboratory and model spectra we thus use step plots rather than smooth lines connecting individual points.

3. Results

3.1. Sensitivity to Geometric Model

[17] Typical apatite grains are hexagonal prisms with a length/radius ratio of about 6 [e.g., *Farley et al.*, 1996]. Under most circumstances in (U-Th)/He thermochronometry a sphere is thought to provide a sufficiently accurate geometric model for bulk diffusion calculations from the hexagonal prism, provided the radius of the model sphere has the same surface to volume ratio as the analyzed prism [*Gautheron and Tassan-Got*, 2010; *Meesters and Dunai*, 2002; *Watson et al.*, 2010]. Current computer codes [*Ketcham*, 2005; *Schildgen et al.*, 2010] assume that this "equivalent sphere" remains an adequate geometric model for computation of

^{4}He/^{3}He spectra as well. However, it is not obvious that this assumption is valid.

[18] To investigate this question we computed model ^{4}He/^{3}He spectra for different geometries. In the absence of analytical solutions for diffusion from a hexagonal prism, we approximate the prism as a cylinder with isotropic diffusion, and with $h/a = 6$. In one set of simulations we assume varying degrees of prior loss (1%, 5%, 10%, and 50%) from an initially uniform profile from the sphere and from the cylinder using the analytical approximations described previously. We also compare spectra for a cylinder and its equivalent sphere that have experienced only α ejection; in this case we use CylmodE for the cylinder. Unlike the previous examples of pure diffusion profiles, this example imposes a true physical dimension, the α ejection length scale of ~20 μm, on the problem. So here we specify a cylindrical geometry measuring 55 by 330 μm (equivalent sphere radius of 76 μm).

[19] Full details of these simulations are listed in Data Set S2.[1] Figure 2a shows results for the pure diffusion profiles. Regardless of the degree of prior release, 1% to 50%, the ^{4}He/^{3}He spectra for the two geometric models are in nearly perfect agreement. This applies throughout the entire range of ΣF^3He. Figure 2b shows the result for the α ejection-only initial profile. In this case the spectra are very slightly offset from each other, but the effect is remarkably small.

[20] Since actual ^{4}He concentration profiles in apatites will lie between the α ejection-only profile and a purely diffused profile, we conclude that these results confirm that the equivalent sphere geometry provides an accurate approximation of the ^{4}He/^{3}He spectrum produced from a cylinder. Given the geometric similarity between a cylinder and a hexagonal prism [*Meesters and Dunai*, 2002; *Watson et al.*, 2010], we further conclude that a sphere provides an adequate geometry for modeling of ^{4}He/^{3}He spectra evolved from natural apatites. The general validity of the equivalent sphere approach has recently been reinforced by *Gautheron and Tassan-Got* [2010].

3.2. Anisotropy

[21] Use of a spherical geometric model for the interpretation of ^{4}He/^{3}He spectra implicitly assumes that He diffusion is crystallographically isotropic. Anisotropic diffusion of He has been observed or predicted in zircon [*Cherniak et al.*, 2009; *Reich et al.*, 2007; *Saadoune et al.*, 2009] and zircon structure orthophosphates [*Farley*, 2007]. In the case of apatite, neither bulk degassing of crystallographically oriented slabs nor profiling of implanted helium [*Cherniak et al.*, 2009; *Farley*, 2000] indicate substantial anisotropy. While this previous work did not set a limit on the possible magnitude of anisotropy, it is probably less than a factor of a few in the temperature range 200–450°C.

[22] To assess how a ^{4}He/^{3}He spectrum would be affected by anisotropic diffusion, we used the CylmodE code to produce spectra for a finite cylinder characterized by an α ejection-only initial ^{4}He profile and dimensions as in section 3.1. We assumed that anisotropy arises only from variations in diffusivity at infinite temperature (D_o), with no distinction in activation energy (E_a), i.e., the ratio of diffusivities along the two axes is a constant with temperature that we vary in our experiments. While these are restrictive assumptions, modeling of scenarios involving variations in activation energy, and/or ^{4}He profiles arising from such variations become extremely dependent on parameter choices and assumed time-temperature path and heating schedule. Our choice of assumption is sufficient to establish conditions under which diffusion anisotropy will noticeably influence ^{4}He/^{3}He spectra.

[23] Computational details and results are given in Data Set S3. Results for the limiting cases of pure radial diffusion and pure axial diffusion are compared with the isotropic case in Figure 3a. Pure radial diffusion yields a profile that is nearly indistinguishable from the isotropic case. This similarity arises from the fact that in the isotropic case ~90% of the helium exits through the cylinder sidewall anyway (CylmodE reports cumulative He loss in each crystallographic direction [*Watson et al.*, 2010]). This 90% is roughly in proportion to the relative surface area of the sidewalls versus the endcaps of the cylinder. Thus eliminating the ~10% exiting the axial faces by adopting pure radial diffusion has almost no impact on the final result.

[24] However the reverse is not true. The ^{4}He/^{3}He spectrum for pure axial diffusion rises much more sharply and flattens earlier than the isotropic or pure radial case. This behavior arises from the fact that the ejection region penetrates just 20 μm into a $h/2$ = 165 μm deep axial profile, or 12% of the entire profile length; in the radial case it penetrates 20 μm into a r = 55 μm profile, or 36% of the length of the profile. Figure 3b shows ^{4}He/^{3}He

[1] Auxiliary materials are available at ftp://ftp.agu.org/apend/gc/2010gc003243.

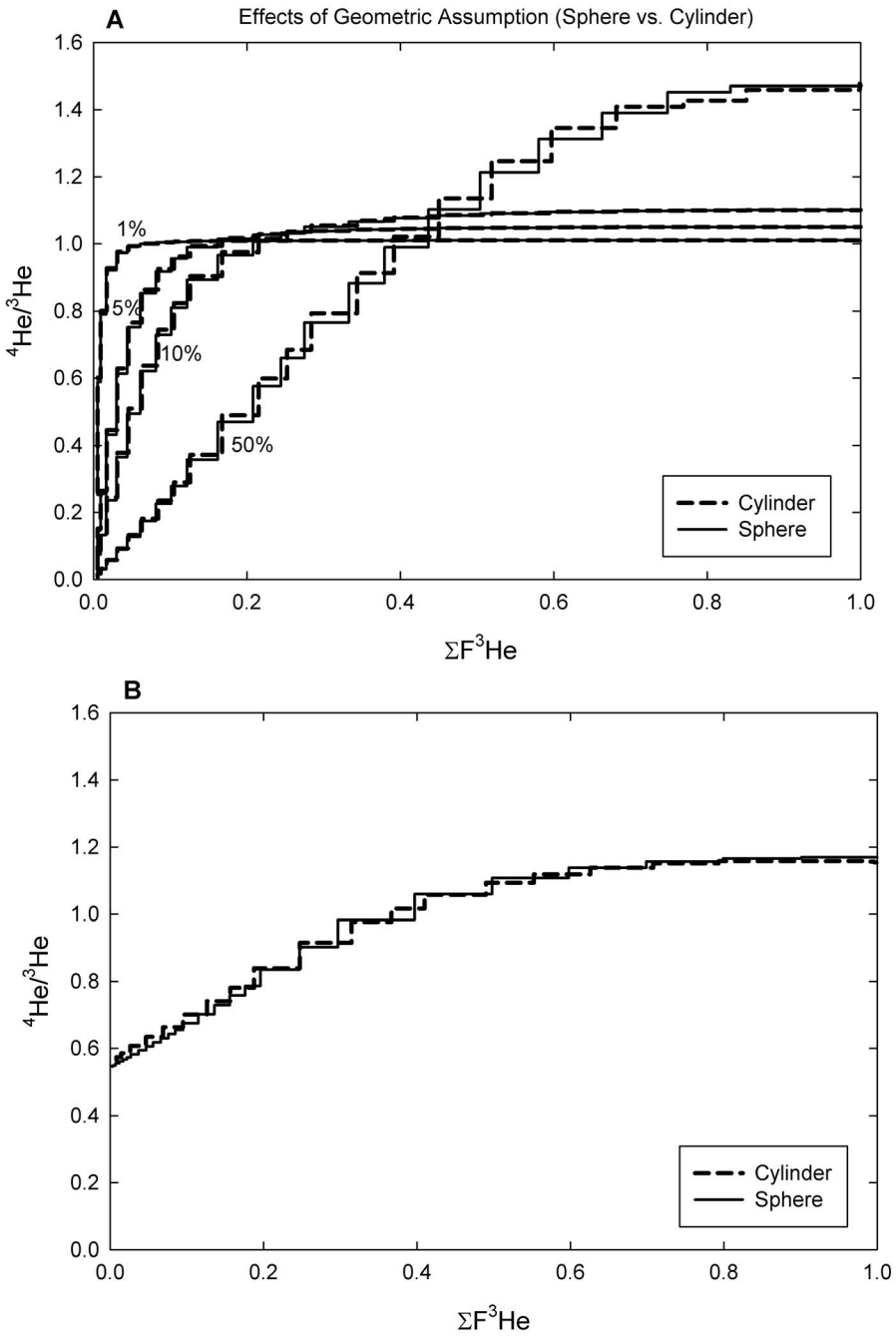

Figure 2. Comparison of spectra obtained from the spherical model with those obtained from the isotropic cylinder model assuming the same initial condition. (a) Results assuming diffusion-only profiles with prior loss of the magnitude indicated by the label beside each curve. (b) Results for α ejection-only profiles. In both cases the cylindrical and spherical models yield nearly identical spectra, validating the use of the spherical geometry when modeling ^{4}He/^{3}He spectra from apatite.

spectra for axial/radial diffusivity ratios of 10 and 50. These spectra indicate that 10-fold higher diffusivity in the axial direction would probably go unnoticed, but 50-fold would certainly be detected. We believe that existing diffusion coefficient measurements rule out even 10-fold axially favored diffusivity in apatite. Furthermore, we note that the common occurrence of measured ^{4}He/^{3}He spectra that lie on the "α ejection-only" boundary for isotropic diffusion from a sphere (e.g., the "Kings River A" sample in Figure 1a as well as several published spectra [*Shuster et al.*, 2005] would be

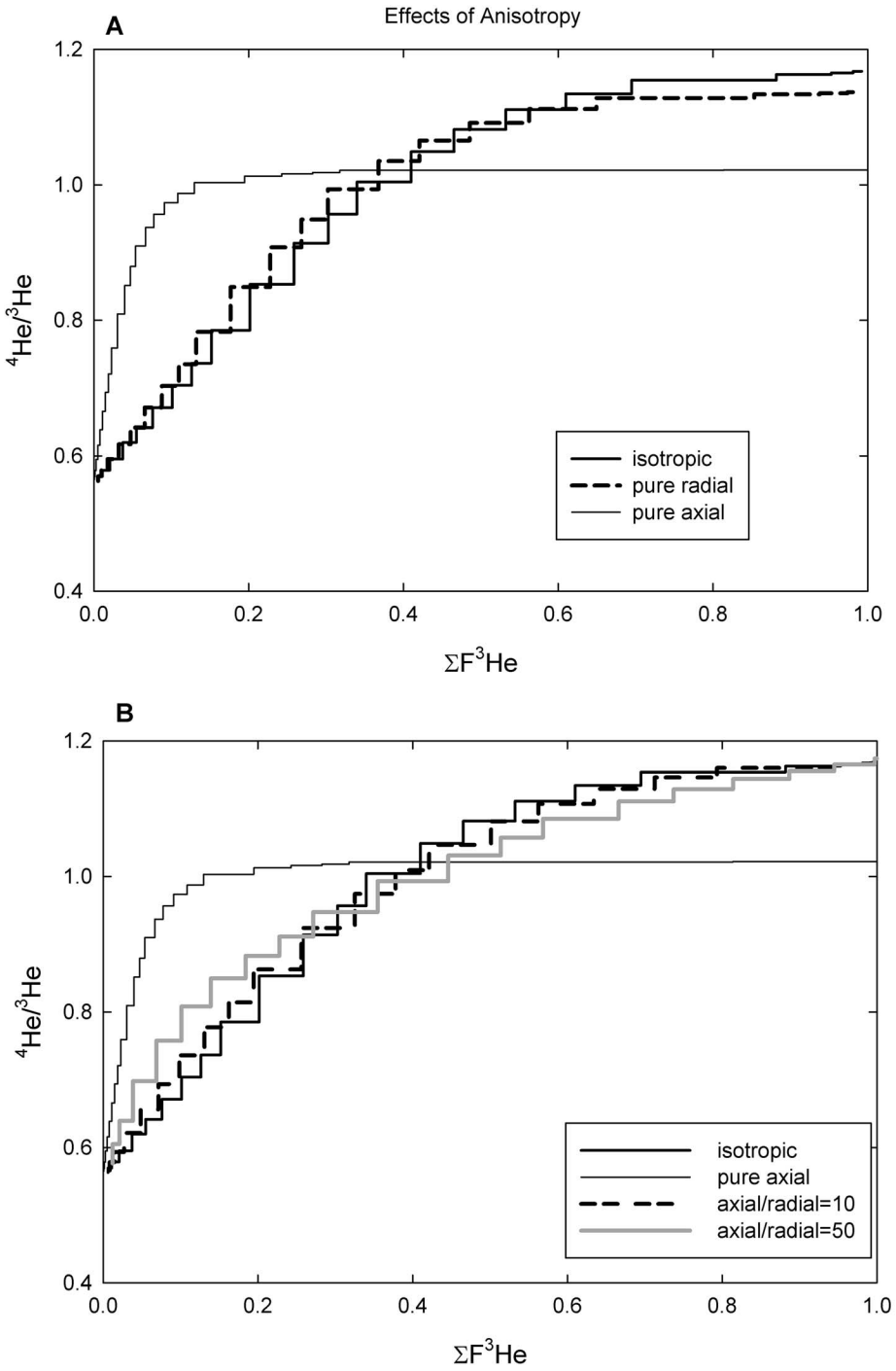

Figure 3. Comparison of ^{4}He/^{3}He spectra obtained from a 330 × 55 μm cylinder assuming varying degrees of anisotropic diffusion from an α ejection-only starting condition. (a) Results for isotropic diffusion, pure axial diffusion, and pure radial diffusion. While pure axial diffusion yields a very different ^{4}He/^{3}He spectrum compared to the isotropic case, pure radial diffusion is almost indistinguishable from the isotropic case. (b) Demonstration that ^{4}He/^{3}He spectra become noticeably different from the isotropic case when the ratio of axial to radial diffusion exceeds about 10. Although data are limited, there is no evidence for this magnitude of anisotropy in apatite.

fortuitous if diffusion in apatite is much faster in the axial compared to the radial direction. Thus we conclude that anisotropy is not likely important in generating anomalous apatite $^4He/^3He$ spectra. However, this may be an important consideration were one to apply the $^4He/^3He$ method to zircon.

3.3. Effect of Broken Terminations

[25] In some rock samples it is easy to find whole euhedral apatite crystals readily distinguished by the presence of pointed or rounded terminations on both ends of the prism. In other rocks most or all of the crystals lack one or both of these terminations, and instead have a flat termination perpendicular to the long axis. It is usually impossible to establish whether these missing terminations represent the original growth morphology within the rock, or if instead the grain terminations were broken off, possibly during the mineral separation process. The importance for $^4He/^3He$ thermochronometry is that a grain broken after the natural development of a diffusion profile will have a fraction of its surface characterized by an anomalously "square" concentration profile (higher concentration at the edge). Intuition suggests that the result will be a $^4He/^3He$ spectrum that begins at values higher than an unbroken grain would yield, and that the magnitude of this discrepancy increases with the degree of rounding of the natural ^4He profile.

[26] To quantify this effect, we can model the $^4He/^3He$ spectrum of a crystal with broken terminations and compare it to an unbroken equivalent in the following manner. We wish to investigate the most extreme effect of breakage, which occurs when the break is located in the uniform concentration interior of the grain. This gives the "broken" surface the maximum possible concentration contrast with the natural surfaces.

[27] To develop this initial condition for a pure diffusion profile (no α ejection) we can use the approximations for diffusion from an anisotropic cylinder. We again assume $h/a = 6$. In the prior release step, we set the axial diffusion coefficient to zero and pick a release coordinate that causes 10% loss. This creates a starting condition for the simulated step heat experiment in which both ends of the prism are characterized by a square concentration profile for ^4He, while the radial edges have very low concentrations. For the simulated stepwise degassing, the diffusivity is assumed isotropic. For the unbroken (reference) case, we repeat the same prior loss simulation in terms of radial release coordinate, but with isotropic diffusion. Because the radial and axial components of the diffusive loss interact very little at this degree of degassing (see *Watson et al.* [2010] for a discussion), we wind up with a nearly identical radial concentration profile and an appropriately rounded axial profile. We then apply the same simulated stepwise degassing schedule. For both the broken and unbroken cases, ^3He diffusivity is assumed isotropic, and no prior release step is used.

[28] Details of this simulation are listed in Data Set S4 and the resulting $^4He/^3He$ spectra are shown in Figure 4a. As expected, $^4He/^3He$ spectra evolved from grains with broken terminations start out with anomalously high $^4He/^3He$ ratios, about 0.17 versus values of nearly zero expected in the first step of an unbroken crystal. This initial value is about what one would predict based on surface area alone: the $h/a = 6$ cylinder has 14% of its surface area in the endcaps, so in the limit of the very first ^4He released we expect a mixture of 14% helium with concentration unity from the endcaps and 86% with concentration zero from the cylinder sidewalls. The slightly higher value actually obtained from the broken grains reflects the fact that the first step in this example interrogates a finite depth, rather than solely the crystal surface.

[29] Indeed a comparison of the model spectra with one obtained by simply assuming a linear combination consisting of 86% of the $^4He/^3He$ ratio of the unbroken crystal with 14% of a $^4He/^3He$ ratio of unity matches the entire spectrum remarkably well, as illustrated for the 25% prior release case (Figure 4b). This demonstrates the relative insignificance of diffusion out the ends of the prism. We can take advantage of this similarity to estimate the consequences of breakage for an α ejection-only profile. Figure 4a shows the results of 86% of the cylindrical α ejection-only profile and 14% $^4He/^3He = 1$.

[30] The effects shown in Figure 4 assume that both ends of the prism are broken. In our experience this is far less common than a single (possibly) broken termination. Thus a more likely case to be encountered is analysis of a crystal with a single broken termination. Such a crystal would yield a $^4He/^3He$ spectrum that plots halfway between the two curves in Figure 4a. While there is certainly an effect arising from analyses of a grain with a broken termination, it is relatively small. The maximum effect occurs in highly rounded profiles. While it is desirable to avoid grains with broken ends, it may be possible to use such grains without introducing large errors.

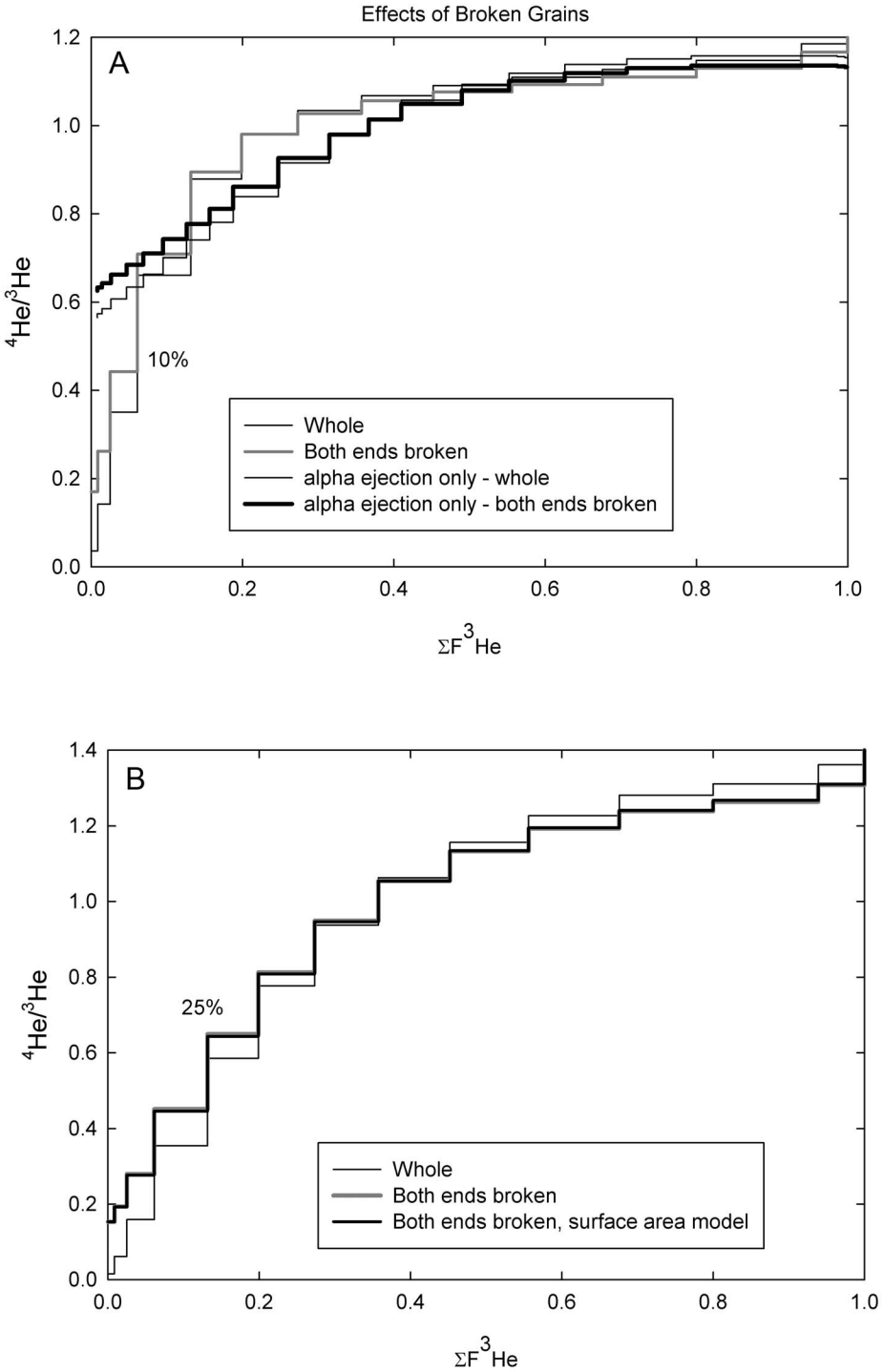

Figure 4. Simulation of ^{4}He/^{3}He spectra from an apatite with two recently broken terminations, modeled as a cylinder. (a) Results for both 10% prior loss and an α ejection-only starting condition. The recently broken terminations are assumed to have experienced no diffusive loss. For both initial conditions the simulation with broken terminations yields a ^{4}He/^{3}He spectrum with initially higher ratios, reflecting the larger contribution of ^{4}He from the cylinder ends. (b) Similar data for the case of 25% prior release compared to a model based on the relative surface areas of the cylinder ends versus the cylinder sidewall.

3.4. Effects of Zonation

[31] Spatial heterogeneity in parent nuclide distribution within an apatite crystal has consequences for bulk (U-Th)/He ages both because it compromises the α ejection correction [*Farley et al.*, 1996; *Hourigan et al.*, 2005] and also modifies the ^{4}He concentration distribution on which diffusion acts [*Farley*, 2000; *Meesters and Dunai*, 2002]. Parent heterogeneity must also impact ^{4}He/^{3}He spectra [*Shuster and Farley*, 2004], but in a way that has not yet been quantitatively described. One challenge for assessing the consequences of heterogeneity is that its frequency and magnitude in apatites have not been well documented. Induced fission track maps can provide an indication of U heterogeneity in some apatites, but this method has limited spatial resolution and does not document Th (or Sm) heterogeneity. U and Th concentrations in apatite are almost always too low to measure by electron probe, leaving only SIMS or LA-ICPMS measurements as adequate for the task. To our knowledge such data are not yet available in the literature. As an alternative, more easily measured rare earth elements (e.g., Ce) or cathodoluminescence intensity may suffice as a proxy for *eU* variability [*Dobson et al.*, 2008; *Jolivet et al.*, 2003]. Limited data [*Jolivet et al.*, 2003; K. A. Farley, unpublished data, 2010] suggest that variability in *eU* of a factor of a few may occur in some apatites. An additional factor to recognize is that the distribution of *eU* is not the same as the initial distribution of ^{4}He, owing to the 20 μm stopping distance of the α particle.

[32] The most extreme consequences of *eU* heterogeneity on ^{4}He/^{3}He spectra will occur for profiles which are least modified by diffusion, because diffusion will act to smoothen the production heterogeneity. Intuition also suggests that concentric zonation will yield more dramatic consequences than patchy heterogeneity or sector zoning that gets scrambled together during the He extraction process. In addition the consequences will be greater when the physical dimensions of the zones are large relative to the α ejection length scale (for example, oscillatory zoning of a few μm wavelength will be totally smoothed by α particle redistribution [*Hourigan et al.*, 2005]). Note that the choice of concentric zoning, although perhaps unrealistic, is required by our radially symmetric diffusion model. The recent model of *Gautheron and Tassan-Got* [2010] could be used to relax this assumption.

[33] Given these considerations we arbitrarily chose to model an apatite with r = 75 μm and a factor of 3 zonation in *eU*. The zone boundary was located at 60 μm from the grain center (Figure 5a), which represents the midpoint by volume (i.e., half of the spherical volume occurs within this radius). This source function was then converted to an α particle production function by assuming a 20 μm stopping distance and no diffusion (Figure 5b); this profile was the starting condition for calculating the ^{4}He/^{3}He spectrum. We explicitly assume that the grain is homogeneous in He diffusivity: local radiation damage accumulations in the *eU*-rich zones do not modify diffusivity. Quantitative details are provided in Data Set S5.

[34] As shown in Figure 5c, the ^{4}He/^{3}He spectra for the zoned apatites are quite different from the unzoned spectrum. When the higher concentration is located toward the rim, the spectrum clearly violates the expected behavior for a uniform *eU* distribution: the initial part of the spectrum plots well in the upper forbidden zone, and the spectrum decreases at high ΣF^3He. When the higher concentrations are located in the core of the grain, the spectrum is substantially steeper than the uniform *eU* case, but does not cross into the forbidden zone. Thus this sense of zonation would not be identified as aberrant. In this case inversion of the ^{4}He/^{3}He spectrum for a temperature history would yield a result indicating slower cooling than actually pertained.

[35] Figure 5c also shows results for these same zonation patterns but assuming the initial condition at the start of the ^{4}He/^{3}He experiment arose from a production-diffusion profile evolved during cooling at a rate of 1°C/Ma and using Durango apatite diffusion kinetics [*Farley*, 2000]. In this case diffusion tends to lessen the consequences of parent nuclide zonation. Nevertheless these spectra would yield erroneous constraints on cooling history if interpreted assuming a homogeneous parent distribution. Comparison of these results with the spectrum of aberrant sample Grand Canyon B in Figure 1c suggests this sample may have a high *eU* rim, a fact confirmed by LA-ICPMS measurements (K. A. Farley, unpublished data, 2010).

[36] These models indicate that *eU* zonation at the level likely present in some apatites can produce both clearly aberrant spectra (plotting in the forbidden zone, and with nonmonotonically increasing ^{4}He/^{3}He evolution) as well as spectra that look normal. This observation confirms that zonation is a potentially serious source of error in ^{4}He/^{3}He

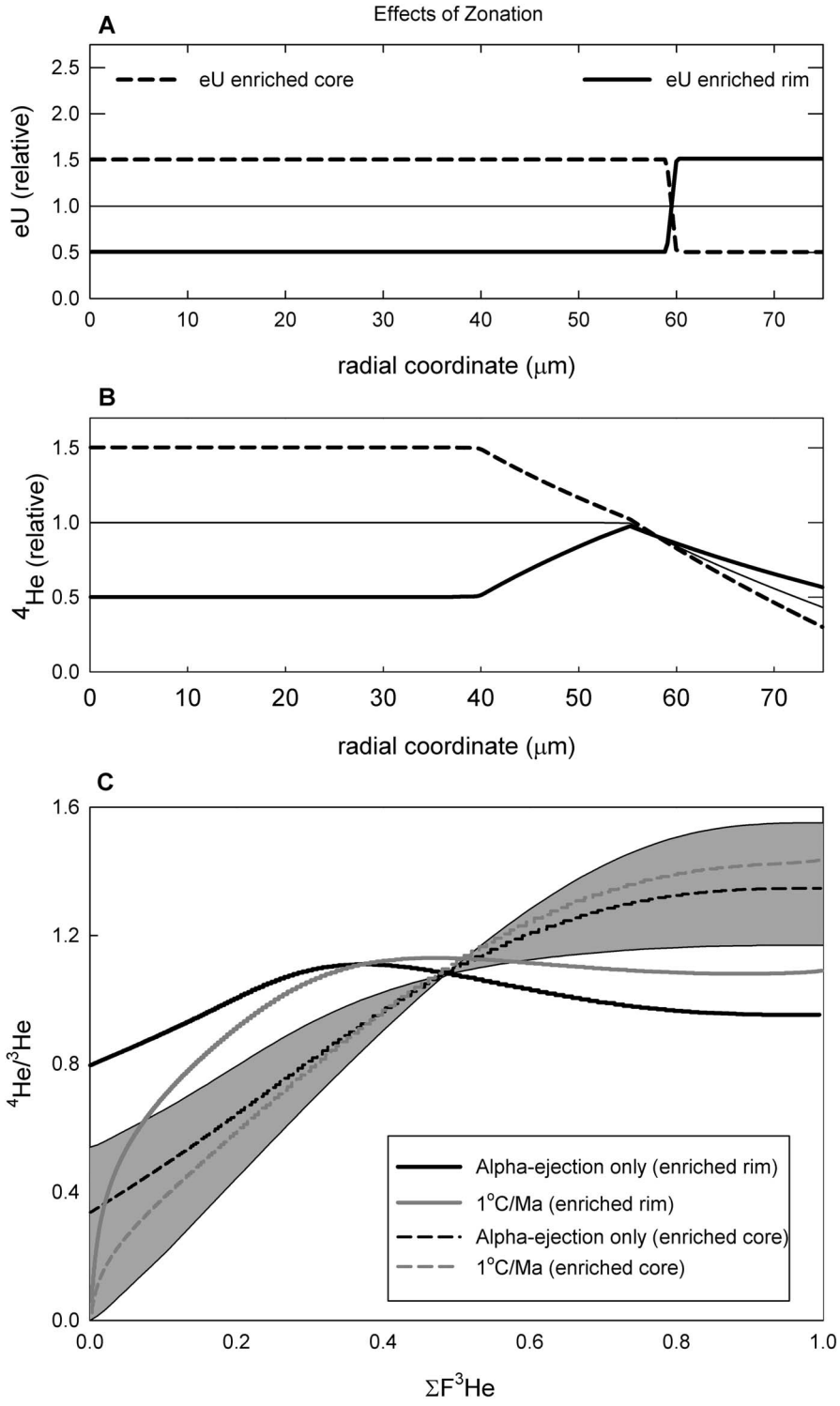

Figure 5. Simulation of ^{4}He/^{3}He spectra for 75 μm radius spherical grains concentrically zoned in eU. (a) The two different eU zonation patterns assumed (factor of 3 contrast and factor of 1/3 contrast between rim and core). (b) The resulting distribution of ^{4}He within these grains following α redistribution and ejection but assuming no diffusive loss (fine solid line is the no zonation reference case). (c) The ^{4}He/^{3}He spectra for the two zonation styles compared to the allowed region shown in Figure 1. Two cooling scenarios are illustrated, one assuming no diffusion (α ejection only) and the other starting with a ^{4}He distribution created by a constant cooling rate of 1°C/Ma (see section 3.4 for details). The grain with the enriched rim plots in the forbidden region regardless of cooling scenario. In contrast the grain with the enriched core yields an acceptable spectrum in both cooling scenarios.

thermochronometry and suggests that further investigation of zonation of U and Th in apatites, especially those subjected to ^{4}He/^{3}He analysis, is warranted. Implantation of alpha particles from high *eU* neighbors [*Spiegel et al.*, 2009] would be expected to produce spectra broadly similar to the rim-enriched model in Figure 5.

3.5. Multiple-Crystal Aliquots: ^{4}He/^{3}He Spectra and ^{3}He Diffusion Parameters

[37] In our early efforts to measure ^{4}He/^{3}He spectra [*Shuster and Farley*, 2004; *Shuster et al.*, 2005] we aggregated multiple crystals into a single stepwise degassing analysis. This was motivated mainly by the desire to obtain enough He for a minimal blank correction. While the mass 3 blank is usually unimportant even for small single crystals, the mass 4 blank can be a significant fraction of the total signal, especially for low eU apatites and/or those with low (U-Th)/He ages.

[38] There are two assumptions that must be met to obtain a meaningful ^{4}He/^{3}He spectrum from an aggregate of crystals: each crystal must have a similar ^{4}He concentration profile, and each must have equivalent He diffusivity during each step of the degassing analysis. Note that these two assumptions are closely related because the ^{4}He concentration profile reflects the crystal's diffusivity in nature. Although aggregates of crystals yield reproducible He diffusivities in the laboratory, we are not aware of any work establishing the degree of variability in He diffusivity among individual apatite crystals from a single rock. In addition, recent work [*Shuster and Farley*, 2009; *Shuster et al.*, 2006] shows that He diffusivity varies with accumulated radiation damage, making these assumptions suspect if crystals vary in eU concentration. Thus it is worth exploring the consequences of differing He diffusivity among crystals aggregated for a ^{4}He/^{3}He run.

[39] The goal of our quantitative model is to compare the ^{4}He/^{3}He spectrum obtained on the aggregate with the spectrum that would be obtained on the crystals individually. Here we assumed isotropic diffusion in a cylinder with $h/a = 1$. We would obtain indistinguishable results assuming spherical geometry. To keep matters simple, we make the following assumptions:

[40] 1. The aggregate consists of two crystals of equivalent mass, referred to as A and B.

[41] 2. Both crystals have exactly the same normalized ^{4}He concentration profile, and that profile is either uniform or the result of 25% prior loss.

[42] 3. The crystals differ in absolute ^{4}He concentration by a factor of x, where $x = C_A/C_B$ and can have values of 1/3, 1, or 3. The crystals have the same ^{3}He concentration.

[43] 4. The crystals differ in diffusivity by a constant factor of 2 at all temperatures, i.e., $D_A/D_B = 2$. We assume an activation energy of 138 kJ/mol and $\ln(D_o/a^2)$ values of 13.6 and 14.3 for crystals A and B, respectively. These values are typical of Durango apatite and correspond to closure temperatures of 70 and 66°C (i.e., they differ by only a small amount).

[44] An arbitrary prograde stepwise heating schedule was assumed. The fraction of ^{3}He and ^{4}He released in each step were computed for each crystal, and summed to get the aggregated yields. The aggregated yields were used to compute the aggregate normalized ^{4}He/^{3}He spectrum. In addition the fractional yield data for ^{3}He were used to compute a diffusion Arrhenius plot following the equations of *Fechtig and Kalbitzer* [1966] recomputed for cylindrical geometry using *Watson et al.* [2010, equation 49]. As we will show, this plot is useful because it demonstrates that the Arrhenius array obtained from an aggregate is sensitive to intercrystal heterogeneity in diffusivity. Full details and results are listed in Data Set S6.

[45] In the first set of simulations we considered an initially uniform ^{4}He distribution, and varied C_A/C_B. Results are shown in Figure 6a. When $C_A/C_B = 1$, the normalized ^{4}He/^{3}He spectrum of the aggregate is uniform at unity, and thus is identical to the spectra from the individual crystals. However, when $C_A/C_B = 3$, the aggregate spectrum is extremely different: it has a strong positive slope, and deviates from unity by up to ~40%. This arises from the fact that the initial release in the aggregate is dominated by the less retentive and lower ^{4}He (and ^{4}He/^{3}He) crystal, while the final steps are dominated by the more retentive and high ^{4}He (and ^{4}He/^{3}He) crystal. A mirror image of this profile is obtained when $C_A/C_B = 1/3$ for exactly the same reason.

[46] Figure 6b shows similar results for the case of 25% prior loss. The same effect is seen: when the less retentive crystal has more ^{4}He, the profile initially overestimates the ^{4}He/^{3}He ratio, then at high ΣF^3He it underestimates it, and vice versa.

[47] While our modeling in Figure 6 considered variations only in D_o/a^2 and not in activation

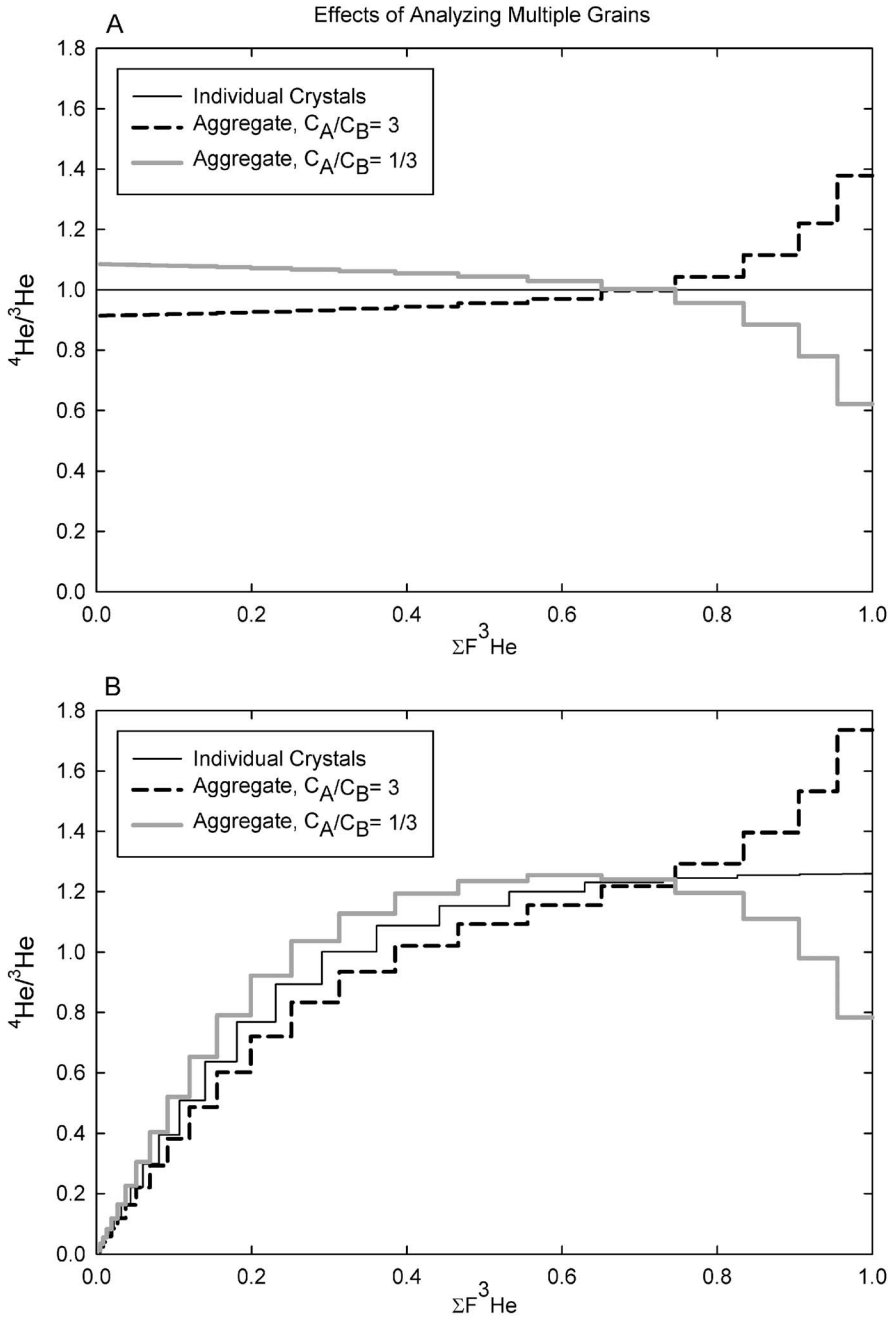

Figure 6. Simulated $^4He/^3He$ spectra for an aggregate of two crystals that differ by a factor of 2 in diffusivity (D_A/D_B = 2) and have relative concentrations C_A/C_B. (a) Results for a uniform initial profile and (b) results assuming 25% prior diffusive loss. Regardless of initial condition the aggregate yields a $^4He/^3He$ spectrum that differs from the spectrum that would be obtained on either crystal individually. This distinction arises because the less retentive grain gives up more of its helium in the early steps, while the more retentive grain dominates the later steps. This simulation argues strongly against analyzing multigrain aggregates for $^4He/^3He$.

energy, the same general pattern would be seen when both parameters vary: the relative contributions from the two crystals will differ in each step, so the aggregate $^4He/^3He$ spectrum does not accurately represent the spectrum in the individual crystals. The characteristic signature of this effect is sharply anomalous deviations in $^4He/^3He$ at high ΣF^3He, either to low or high values. In addition, if temperatures are cycled during the experiment, it is possible that the relative contributions from the two

crystals will reverse, leading to positive or negative "spikes" in the spectrum. ^{4}He/^{3}He spectra with either of these behaviors are readily identified as ill behaved. Positive or negative spikes cannot be produced by stepwise degassing of a simple production-diffusion distribution, and the deviations at high ΣF^3He will in general plot outside the allowed region (Figure 1).

[48] Each of these patterns has been observed in our unpublished early experiments using multiple crystal aggregates. For example, compare Figure 6 with the aberrant Kings River B results in Figure 1c. We suspect that this is the origin of many of the discrepant ^{4}He/^{3}He spectra we have obtained on multiple crystal aliquots. Clearly it is necessary to analyze ^{4}He/^{3}He spectra on single crystals. *McDougall and Harrison* [1988] present similar considerations when measuring Ar/Ar age spectra of polyminerallic aggregates.

[49] Figure 7 presents an additional observation that arises from this modeling: even small differences in diffusivity among the crystals can yield an aggregate Arrhenius plot that does not accurately capture the diffusion parameters of either crystal. Figure 7 shows Arrhenius plots obtained from simulated step heat results for ^{3}He as in the previous examples, but for $D_A/D_B = 4$ to make the effect more readily apparent. This corresponds to crystals with closure temperatures of 70 and 61°C. (Note that since we are considering only ^{3}He, neither the initial ^{4}He profile nor the absolute ^{4}He concentration matter for this example.) In the case of a monotonically increasing temperature schedule (Figure 7a), the result is an Arrhenius array which lies between that of the two individual crystals. As the experiment proceeds the less retentive crystal depletes more rapidly than the more retentive crystal, causing the array to curve downward toward the more retentive crystal's diffusion characteristics. This behavior is analogous to the effect described by *Lovera et al.* [1991] and by *Fulda and Lippolt* [2000] for the case of a distribution in diffusion domain radii in an analyzed sample.

[50] Figure 7b shows the results of making the same assumptions as in Figure 7a, but using different heating schedules. The filled squares depict the case of a relatively small number of steps concentrated at the high end of the original temperature schedule. Here the aggregate Arrhenius array looks roughly linear (arrow shown), yet it would indicate an activation energy and closure temperature significantly lower than either crystal being analyzed. The second simulation (filled symbols) shows the same effect revealed by a cycled step heat experiment: the Arrhenius array defines a declining zigzag pattern. The point here is that the Arrhenius parameters of an aggregate need not be the mean of the crystals that compose the aggregate. Furthermore, a downward curving and/or zigzag array are evidence for this phenomenon.

[51] These effects provide one possible explanation for the recent observation that ^{3}He-based diffusivities become unreliable (low activation energy, zigzag Arrhenius array) in highly radiation damaged samples [*Shuster and Farley*, 2009]. Variability in the *eU* concentration and hence the degree of radiation damage among crystals could yield varying diffusivities among grains in the aliquot. Experiments to establish the He diffusivity on individual crystals of these samples is needed to evaluate this possibility.

4. Conclusions

[52] Numerical simulations demonstrate that ^{4}He/^{3}He spectra evolved from a cylinder with isotropic He diffusion and its equivalent spherical representation are nearly indistinguishable, an observation that justifies the use of the simpler spherical approximations. In contrast, ^{4}He/^{3}He spectra evolved from a cylinder with strongly anisotropic diffusion ($D_{axial}/D_{radial} > \sim 10$) are distinctly different from the spherical case. While this degree and sense of He diffusion anisotropy may occur in zircons, it can be ruled out in apatite on the basis of laboratory diffusion experiments [*Farley*, 2000; *Cherniak et al.*, 2009] and the good match of some observed ^{4}He/^{3}He spectra to the spherical α ejection-only ^{4}He/^{3}He bound (e.g., Figure 1a). These observations justify the assumptions used in available interpretive models of (U-Th)/He ages (e.g., HeFTy [*Ketcham*, 2005]) and ^{4}He/^{3}He spectra [e.g., *Schildgen et al.*, 2010].

[53] These models of necessity assume that the analyzed grain is entirely unbroken, yet many rocks yield apatites which have terminations suggesting recent breakage. Because recently exposed surfaces will have experienced less diffusive loss, they will bias initial steps in a ^{4}He/^{3}He experiment toward higher ratios. The magnitude of the effect is roughly proportional to the fraction of surface area recently exposed. In the case of breakage of grain terminations (which are a small fraction of the entire grain surface), the consequences are sufficiently small as to be routinely ignored. However, apatites that have large chips or significant abrasion

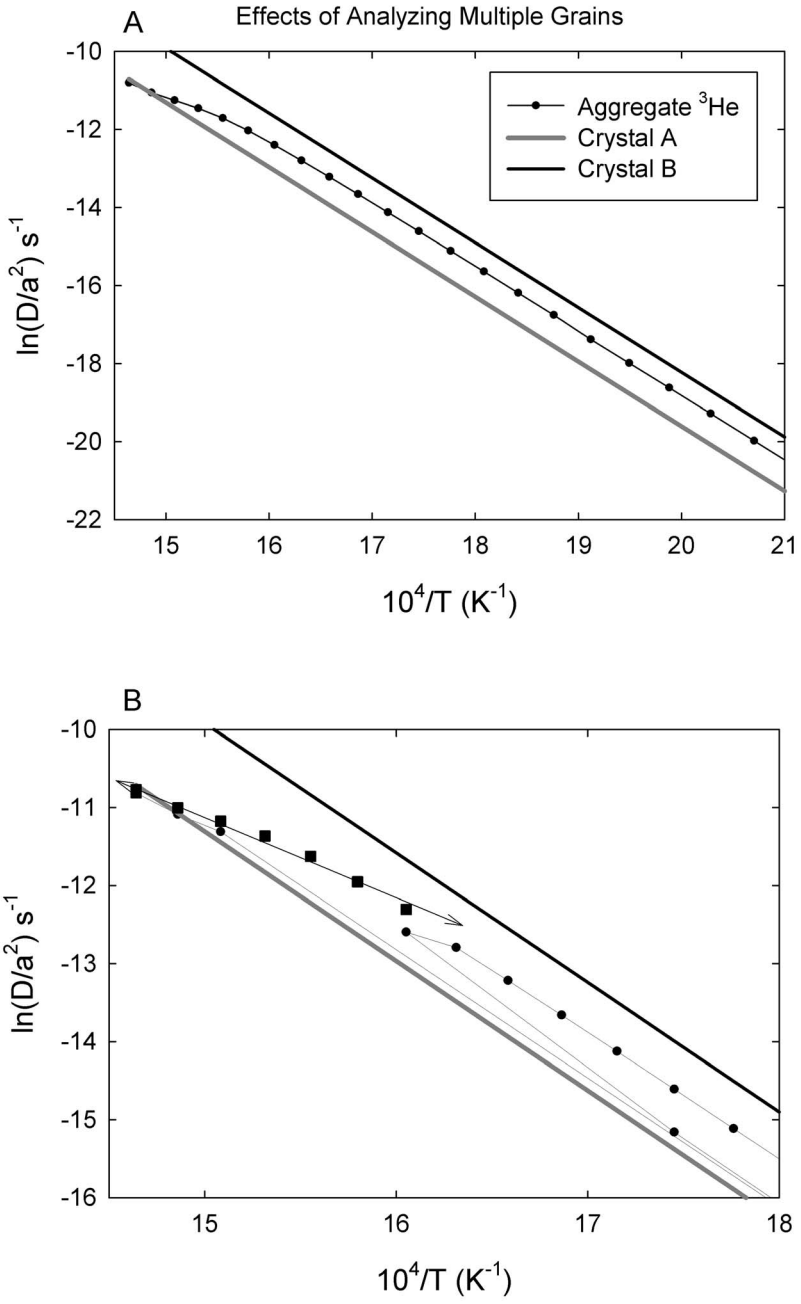

Figure 7. Arrhenius plots simulated for a two-crystal aggregate with $D_A/D_B = 4$ and a uniform and identical concentration of helium in the two crystals. (a) Comparison of the results obtained on the aggregate to the diffusivities assumed for the individual grains, assuming a monotonic heating schedule spanning a large temperature range. The aggregate diffusivity is curved because it is initially dominated by the less retentive grain, but as the experiment proceeds this grain becomes depleted and the diffusivity declines toward that of the more retentive grain. (b) Comparison starting with the same assumptions as in Figure 7a but using two different heating schedules described in section 3.5. These simulations show that mixtures of grains with different diffusivities analyzed together need not yield accurate diffusion parameters (as suggested by arrow in Figure 7b). The telltale signs of this effect are a curved Arrhenius array and, for cycled experiments, a declining zigzag pattern.

or chemical pitting produced late in the grain's history may yield unacceptably biased ^{4}He/^{3}He spectra.

[54] In contrast to these relatively minor effects, modeling reveals two factors of great significance for producing and accurately interpreting ^{4}He/^{3}He spectra. First, simultaneous analysis of multiple crystals in a ^{4}He/^{3}He analysis can yield wildly erroneous spectra given even modest variation in He diffusivity between grains. Such experiments can also yield invalid ^{3}He diffusion Arrhenius parameters. This problem is readily solved by analysis of individual crystals provided sufficient signal can be obtained to overcome analytical blanks. A bigger problem is presented by inhomogeneous parent nuclide distribution. Modeling shows that concentric zonation at the level of a factor of 3 can yield ^{4}He/^{3}He spectra that in the best case can be identified as aberrant, and in the worst case look acceptable but would not yield accurate time-temperature histories if interpreted assuming homogeneity. This observation suggests that apatites subjected to ^{4}He/^{3}He analysis be evaluated for zonation, either by characterizing the population from which the selected apatite is drawn, or even better, by analysis of parent nuclide variability in the analyzed grain after the stepwise degassing ^{4}He/^{3}He analysis is completed. The degree to which parent nuclide heterogeneity is a common problem is difficult to evaluate in the near total absence of detailed measurements in apatite.

Acknowledgments

[55] This work was supported by NSF grants to K.A.F. (EAR-0738627), D.L.S. (EAR-0738474), and E.B.W. (EAR-0440228 and EAR-0738843). D.L.S. also acknowledges the Ann and Gordon Getty Foundation.

References

Boyce, J. W., and K. V. Hodges (2005), U and Th zoning in Cerro de Mercado (Durango, Mexico) fluorapatite: Insights regarding the impact of recoil redistribution of radiogenic He-4 on (U-Th)/He thermochronology, *Chem. Geol.*, *219*(1–4), 261–274, doi:10.1016/j.chemgeo.2005.02.007.

Cherniak, D. J., E. B. Watson, and J. B. Thomas (2009), Diffusion of helium in zircon and apatite, *Chem. Geol.*, *268*(1–2), 155–166, doi:10.1016/j.chemgeo.2009.08.011.

Colgan, J. P., D. L. Shuster, and P. W. Reiners (2008), Two-phase Neogene extension in the northwestern Basin and Range recorded in a single thermochronology sample, *Geology*, *36*(8), 631–634, doi:10.1130/G24897A.1.

Dobson, K. J., F. M. Stuart, T. J. Dempster, and EIMF (2008), U and Th zonation in Fish Canyon Tuff zircons: Implications for a zircon (U-Th)/He standard, *Geochim. Cosmochim. Acta*, *72*(19), 4745–4755, doi:10.1016/j.gca.2008.07.015.

Farley, K. A. (2000), Helium diffusion from apatite: General behavior as illustrated by Durango fluorapatite, *J. Geophys. Res.*, *105*(B2), 2903–2914, doi:10.1029/1999JB900348.

Farley, K. A. (2007), He diffusion systematics in minerals: Evidence from synthetic monazite and zircon structure phosphates, *Geochim. Cosmochim. Acta*, *71*(16), 4015–4024, doi:10.1016/j.gca.2007.05.022.

Farley, K. A., R. A. Wolf, and L. T. Silver (1996), The effects of long alpha-stopping distances on (U-Th)/He ages, *Geochim. Cosmochim. Acta*, *60*, 4223–4229, doi:10.1016/S0016-7037(96)00193-7.

Fechtig, H., and S. Kalbitzer (1966), The diffusion of argon in potassium-bearing solids, in *Potassium Argon Dating*, compiled by O. A. Schaeffer and J. Zahringer, pp. 68–107, Springer, New York.

Fitzgerald, P., R. Sorkhabi, T. Redfield, and E. Stump (1995), Uplift and denudation of the central Alaska Range: A case study in the use of apatite fission track thermochronology to determine absolute uplift parameters, *J. Geophys. Res.*, *100*, 20,175–20,191, doi:10.1029/95JB02150.

Fulda, C., and H. J. Lippolt (2000), Diffusion coefficients of noble gases in natural minerals: An apparent experimental time dependence caused by domain size spectra, *Math. Geol.*, *32*(1), 31–47, doi:10.1023/A:1007550600841.

Gautheron, C., and L. Tassan-Got (2010), A Monte Carlo approach to diffusion applied to noble gas/helium thermochronology, *Chem. Geol.*, *273*(3–4), 212–224, doi:10.1016/j.chemgeo.2010.02.023.

Hourigan, J. K., P. W. Reiners, and M. T. Brandon (2005), U-Th zonation-dependent alpha-ejection in (U-Th)/He chronometry, *Geochim. Cosmochim. Acta*, *69*(13), 3349–3365, doi:10.1016/j.gca.2005.01.024.

Jolivet, M., T. Dempster, and R. Cox (2003), Distribution of U and Th in apatites: Implications for U-Th/He thermochronology, *C. R. Geosci.*, *335*(12), 899–906, doi:10.1016/j.crte.2003.08.010.

Ketcham, R. A. (2005), Forward and inverse modeling of low-temperature thermochronometry data, in *Low-Temperature Thermochronology: Techniques, Interpretations, and Applications*, *Rev. Mineral. Geochem.*, vol. 58, pp. 275–314, doi:10.2138/rmg.2005.58.11, Mineral. Soc. of Am., Washington, D. C.

Lovera, O., F. Richter, and T. Harrison (1991), Diffusion domains determined by ^{39}Ar released during step heating, *J. Geophys. Res.*, *96*, 2057–2069, doi:10.1029/90JB02217.

McDougall, I., and T. M. Harrison (1988), *Geochronology and Thermochronology by the ^{40}Ar/^{39}Ar Method*, Oxford Univ. Press, New York.

Meesters, A., and T. J. Dunai (2002), Solving the production-diffusion equation for finite diffusion domains of various shapes: Part 1. Implications for low-temperature (U-Th)/He thermochronology, *Chem. Geol.*, *186*(3–4), 333–344, doi:10.1016/S0009-2541(01)00422-3.

Reich, M., R. C. Ewing, T. A. Ehlers, and U. Becker (2007), Low-temperature anisotropic diffusion of helium in zircon: Implications for zircon (U-Th)/He thermochronometry, *Geochim. Cosmochim. Acta*, *71*, 3119–3130, doi:10.1016/j.gca.2007.03.033.

Saadoune, I., J. A. Purton, and N. H. de Leeuw (2009), He incorporation and diffusion pathways in pure and defective zircon $ZrSiO_4$: A density functional theory study, *Chem. Geol.*, *258*(3–4), 182–196, doi:10.1016/j.chemgeo.2008.10.015.

Schildgen, T. F., G. Balco, and D. L. Shuster (2010), Canyon incision and knickpoint propagation recorded by apatite ^{4}He/^{3}He thermochronometry, *Earth Planet. Sci. Lett.*, *293*(3–4), 377–387, doi:10.1016/j.epsl.2010.03.009.

Shuster, D. L., and K. A. Farley (2004), ^{4}He/^{3}He thermochronometry, *Earth Planet. Sci. Lett.*, *217*(1–2), 1–17, doi:10.1016/S0012-821X(03)00595-8.

Shuster, D. L., and K. A. Farley (2005), ^{4}He/^{3}He thermochronometry: Theory, practice, and potential complications, in *Low-Temperature Thermochronology: Techniques, Interpretations, and Applications*, *Rev. Mineral. Geochem.*, vol. 58, pp. 181–203, doi:10.2138/rmg.2005.58.7, Mineral. Soc. of Am., Washington, D. C.

Shuster, D. L., and K. A. Farley (2009), The influence of artificial radiation damage and thermal annealing on helium diffusion kinetics in apatite, *Geochim. Cosmochim. Acta*, *73*(1), 183–196, doi:10.1016/j.gca.2008.10.013.

Shuster, D. L., K. A. Farley, J. M. Sisterson, and D. S. Burnett (2004), Quantifying the diffusion kinetics and spatial distributions of radiogenic ^{4}He in minerals containing proton-induced ^{3}He, *Earth Planet. Sci. Lett.*, *217*(1–2), 19–32, doi:10.1016/S0012-821X(03)00594-6.

Shuster, D. L., T. A. Ehlers, M. E. Rusmore, and K. A. Farley (2005), Rapid glacial erosion at 1.8 Ma revealed by ^{4}He/^{3}He thermochronometry, *Science*, *310*(5754), 1668–1670, doi:10.1126/science.1118519.

Shuster, D. L., R. M. Flowers, and K. A. Farley (2006), The influence of natural radiation damage on helium diffusion kinetics in apatite, *Earth Planet. Sci. Lett.*, *249*(3–4), 148–161, doi:10.1016/j.epsl.2006.07.028.

Spiegel, C., B. Kohn, D. Belton, Z. Berner, and A. Gleadow (2009), Apatite (U-Th-Sm)/He thermochronology of rapidly cooled samples: The effect of He implantation, *Earth Planet. Sci. Lett.*, *285*(1–2), 105–114, doi:10.1016/j.epsl.2009.05.045.

Wagner, G., and G. Reimer (1972), Fission track tectonics: The tectonic interpretation of fission track apatite ages, *Earth Planet. Sci. Lett.*, *14*, 263–268, doi:10.1016/0012-821X(72)90018-0.

Watson, E. B., K. H. Wanser, and K. A. Farley (2010), Anisotropic diffusion in a finite cylinder, with geochemical applications, *Geochim. Cosmochim. Acta*, *74*(2), 614–633, doi:10.1016/j.gca.2009.10.013.

Wolf, R. A., K. A. Farley, and L. T. Silver (1996a), Helium diffusion and low-temperature thermochronometry of apatite, *Geochim. Cosmochim. Acta*, *60*(21), 4231–4240, doi:10.1016/S0016-7037(96)00192-5.

Wolf, R. A., K. A. Farley, and L. T. Silver (1996b), Assessment of (U-Th)/He thermochronometry: The low-temperature history of the San Jacinto Mountains, *Calif. Geol.*, *25*, 65–68.

Wolf, R. A., K. A. Farley, and D. M. Kass (1998), Modeling of the temperature sensitivity of the apatite (U-Th)/He thermochronometer, *Chem. Geol.*, *148*(1–2), 105–114, doi:10.1016/S0009-2541(98)00024-2.